

Carbon/Molecule/Metal and Carbon/Molecule/Metal Oxide Molecular Electronic Junctions

Rajendra Prasad Kalakodimi, Aletha M. Nowak, and Richard L. McCreery*

Department of Chemistry, The Ohio State University, 100 West 18th Avenue, Columbus, Ohio 43210

Received March 31, 2005. Revised Manuscript Received July 14, 2005

Molecular junctions were fabricated on the basis of a 1.7–4.5 nm thick layer of fluorene (FL) or nitroazobenzene (NAB) covalently bonded to a graphitic pyrolyzed photoresist film (PPF) substrate. The junction was completed with a top contact consisting of metallic Cu, TiO₂, or aluminum(III) oxide (AlOx) and a final layer of Au. The current/voltage behavior of the junctions depended strongly both on the nature of the metal or metal oxide top layers and on the structure of the molecular layer. PPF/NAB/Cu/Au and PPF/FL/Cu/Au junctions were highly conducting, with resistances of 0.3–1.7 Ω cm², depending on the identity and thickness of the molecular layer. Substitution of Cu with either AlOx or TiO₂ caused a large increase in junction resistance by 2–4 orders of magnitude, but also yielded rectifying junctions in the case of PPF/NAB(4.5)/TiO₂(3.1)/Au. For a positive bias (PPF relative to Au) above +2 V, the NAB(4.5)/TiO₂(3.1) junction became highly conductive, apparently due to injection of electrons into the TiO₂ conduction band. PPF/NAB(4.5)/AlOx(3.3)/Au junctions exhibited symmetric *i/V* responses with very low currents, and capacitances consistent with those expected for a parallel plate capacitor with two dielectric layers. However, Raman spectroscopy of the NAB/AlOx junctions showed structural changes under negative bias corresponding to reduction of NAB, despite the absence of significant current flow. The changes were reversible and repeatable provided the bias was between –1.5 and +1.0, but partially irreversible when the bias excursion was negative of –1.5 V. Combined with a previous spectroscopic study of PPF/NAB/TiO₂/Au junctions, the results imply a rectification mechanism based on electron transport through the NAB LUMO and the TiO₂ conduction band, and possibly a Coulombic barrier resulting from reduction of the NAB in the molecular junction.

Introduction

Many metal/molecule/metal molecular electronic junctions have been reported,¹ most commonly based on self-assembled monolayer (SAM)^{2–9} and Langmuir–Blodgett^{10–13} structures. Of particular interest are those exhibiting rectification and conductance switching,^{14–16} due in part to potential

applications in microelectronics. We have investigated molecular junctions based on covalent bonding to a graphitic carbon substrate, with a metal^{17–19} or metal oxide^{20–22} top contact. The substrate is made by pyrolysis of commercial photoresist (pyrolyzed photoresist film, or PPF), and resembles a very flat (rms < 0.5 nm) form of glassy carbon, with a resistivity of 0.005 Ω cm.^{23,24} The molecular layer is bonded to the PPF by a covalent C–C bond, made by electrochemical reduction of a diazonium reagent, and the resulting mono- or multilayer has been characterized by

* To whom correspondence should be addressed. Phone: (614) 292-2021. E-mail: mcreery.2@osu.edu.

- (1) McCreery, R. *Chem. Mater.* **2004**, *16*, 4477.
- (2) Zhou, C.; Deshpande, M. R.; Reed, M. A.; Jones, L.; Tour, J. M. *Appl. Phys. Lett.* **1997**, *71*, 611.
- (3) Chang, S.-C.; Li, Z.; Lau, C. N.; Larade, B.; Williams, R. S. *Appl. Phys. Lett.* **2003**, *83*, 3198.
- (4) Slowinski, K.; Majda, M. *J. Electroanal. Chem.* **2000**, *491*, 139.
- (5) Holmlin, R. E.; Haag, R.; Chabinyk, M. L.; Ismagilov, R. F.; Cohen, A. E.; Terfort, A.; Rampi, M. A.; Whitesides, G. M. *J. Am. Chem. Soc.* **2001**, *123*, 5075.
- (6) Rampi, M. A.; Whitesides, G. M. *Chem. Phys.* **2002**, *281*, 373.
- (7) Haag, R.; Rampi, M. A.; Holmlin, R. E.; Whitesides, G. M. *J. Am. Chem. Soc.* **1999**, *121*, 7895.
- (8) Slowinski, K.; Fong, H. K. Y.; Majda, M. *J. Am. Chem. Soc.* **1999**, *121*, 7257.
- (9) Tran, E.; Rampi, M. A.; Whitesides, G. M. *Angew. Chem., Int. Ed.* **2004**, *43*, 3835.
- (10) Stewart, D. R.; Ohlberg, D. A. A.; Beck, P. A.; Chen, Y.; Williams, R. S.; Jeppesen, J. O.; Nielsen, K. A.; Stoddart, J. F. *Nano Lett.* **2004**, *4*, 133.
- (11) Chen, Y.; Ohlberg, D. A. A.; Li, X.; Stewart, D. R.; Williams, R. S.; Jeppesen, J. O.; Nielsen, K. A.; Stoddart, J. F.; Olynick, D. L.; Anderson, E. *Appl. Phys. Lett.* **2003**, *82*, 1610.
- (12) Chen, Y.; Jung, G.-Y.; Ohlberg, D. A. A.; Li, X.; Stewart, D. R.; Jeppesen, J. O.; Nielsen, K. A.; Stoddart, J. F.; Williams, R. S. *Nanotechnology* **2003**, *14*, 462.
- (13) Jaiswal, A.; Amaresh, R. R.; Lakshminantham, M. V.; Honciuc, A.; Cava, M. P.; Metzger, R. M. *Langmuir* **2003**, *19*, 9043.

- (14) Collier, C. P.; Jeppesen, J. O.; Luo, Y.; Perkins, J.; Wong, E. W.; Heath, J. R.; Stoddart, J. F. *J. Am. Chem. Soc.* **2001**, *123*, 12632.
- (15) Heath, J. R.; Collier, C. P.; Mattersteig, G.; Raymo, F. M.; Stoddart, J. F.; Wong, E. Electrically Addressable Volatile Non-Volatile Molecular-Based Switching Devices. U.S. Patent 6,198,655, 2001.
- (16) Pease, A. R.; Jeppesen, J. O.; Stoddart, J. F.; Luo, Y.; Collier, C. P.; Heath, J. R. *Acc. Chem. Res.* **2001**, *34*, 433.
- (17) Anariba, F.; Steach, J.; McCreery, R. *J. Phys. Chem. B* **2005**, *109*, 11163.
- (18) Anariba, F.; McCreery, R. L. *J. Phys. Chem. B* **2002**, *106*, 10355.
- (19) Solak, A. O.; Ranganathan, S.; Itoh, T.; McCreery, R. L. *Electrochem. Solid State Lett.* **2002**, *5*, E43.
- (20) McCreery, R.; Dieringer, J.; Solak, A. O.; Snyder, B.; Nowak, A. M.; McGovern, W. R.; DuVall, S. *J. Am. Chem. Soc.* **2004**, *126*, 6200.
- (21) McCreery, R. L.; Dieringer, J.; Solak, A. O.; Snyder, B.; Nowak, A.; McGovern, W. R.; DuVall, S. *J. Am. Chem. Soc.* **2003**, *125*, 10748.
- (22) McGovern, W. R.; Anariba, F.; McCreery, R. *J. Electrochem. Soc.* **2005**, *152*, E176.
- (23) Ranganathan, S. Preparation, Modification and Characterization of a Novel Carbon Electrode Material for Applications in Electrochemistry and Molecular Electronics. Ph.D. Thesis, The Ohio State University, Columbus, OH, 2001.
- (24) Ranganathan, S.; McCreery, R. L. *Anal. Chem.* **2001**, *73*, 893.

Raman spectroscopy,^{25–28} FTIR,^{29,30} XPS,^{28,31,32} AFM,^{30,33–35} and SIMS.³⁶ Carbon-based molecular junctions exhibit current/voltage behavior which depends strongly on the structure and thickness of the molecular layer,^{17,18,37} and in certain cases exhibits strong rectification.^{20–22} The *i/V* behavior is reproducible and robust, with device yields exceeding 80% and endurance of thousands of voltage scans.

In the course of developing carbon/molecule/titanium junctions, we observed a strong dependence of the *i/V* behavior on the residual gas pressure during Ti deposition.^{20–22} The involvement of titanium oxide in junction behavior was investigated by XPS depth profiling, and by comparison of Ti and Cu as metal top contacts. In addition, in situ Raman spectroscopy in functioning carbon/nitroazobenzene(NAB)/titanium oxide/Au junctions revealed that a redox process occurred under applied bias, reducing the molecule and modulating the junction conductivity.²⁶ We proposed that conductance switching was due to injection of electrons into the titanium oxide conduction band under positive bias (PPF relative to Au), which accompanied redox activity in the NAB/titanium oxide layers. The in situ spectroscopy clearly demonstrated structural changes within the junction in the presence of an applied electric field, but the connection between such changes and *i/V* behavior remains to be understood completely.

The current work was undertaken to reveal the connections between structure and *i/V* behavior in carbon/molecule/metal/Au junctions, particularly related to rectification in carbon/NAB/titanium oxide/Au junctions. Cu and aluminum oxide top contacts are compared to titanium oxide to compare conducting and insulating contacts to those of semiconducting titanium oxide. In addition, three molecular layers were compared: an NAB monolayer, an NAB multilayer, and a fluorene (FL) monolayer. Fluorene was chosen as a second molecular structure which differed from NAB in its lack of a nitro or azo group to determine if those entities were determinants of junction electronic behavior. To clearly distinguish various junction designs, the molecular layer thickness and metal thickness will be given where appropriate. For example, PPF/NAB(4.5)/AlOx(3.3)/Au denotes a PPF substrate, a 4.5 nm thick NAB layer, a 3.3 nm thick aluminum(III) oxide layer, and a Au top layer to yield a total metal/metal oxide thickness of 10.0 nm.

Experimental Section

Molecular junctions were fabricated in a cross-junction configuration described previously,¹⁷ with the junction formed at the intersection of a PPF line and a vapor-deposited metal or metal/metal oxide stripe. Insulating, flat substrates of silicon wafers (boron doped, 12–16 Ω cm) with a coating of 1500 Å of silicon nitride (Virginia Semiconductor, Inc.) were cut into 1 cm × 2 cm samples. Cut pieces were sonicated in acetone (Mallinckrodt AR, 99.7%) for 5 min, followed by a 30 s rinse in isopropyl alcohol (Sigma-Aldrich, 99.5%) and Nanopure water (18 MΩ cm, Barnstead), and then the samples were dried under a stream of argon gas. PPF films, which form the bottom contact for the molecular junctions, were prepared as described previously.^{18,24,38} The clean silicon nitride pieces were spin coated with the positive photoresist AZP4330-RS (AZ Electronic Materials, Somerville, NJ), soft-baked at 90 °C for 20 min, and then cooled to room temperature before photolithography. Individual samples were then placed under a lithographic contact mask (Photo Sciences, Inc., Torrance, CA) with a pattern of four stripes 1 mm in width. A mercury arc lamp (model 68810, Oriel Corp., Stratford, CT) operating at 350 W was used to expose the photoresist to soft UV radiation for 120 s. Immediately after UV exposure, the samples were submerged into a 1:4 (v/v) solution of photoresist developer (AZ 400K, AZ Electronic Materials) in Nanopure water for 20–30 s, then rinsed with Nanopure water, and dried with argon. Pyrolysis was carried out as described previously at 1000 °C for 1 h in the presence of forming gas (95% nitrogen and 5% hydrogen). Prior to surface modification, the PPF samples were rinsed with acetonitrile (Sigma-Aldrich, 99.5%) which was treated with activated carbon filtered with 0.2 μm nylon filters (Millipore) prior to surface modification.

Electrochemical derivatization was performed with a BAS 100 W potentiostat (Bioanalytical Systems, West Lafayette, IN), as described previously.^{21,33} An electrolyte solution consisting of a 1 mM concentration of the corresponding diazonium salt dissolved in acetonitrile solution with 0.1 M tetrabutylammonium tetrafluoroborate ((TBA)BF₄; Sigma-Aldrich, 99.5%) was used for the electrochemical derivatization. A Ag/Ag⁺ (0.01 M AgNO₃ and 0.1 M TBABF₄ in acetonitrile) reference electrode (Bioanalytical Systems), calibrated with ferrocene to be +0.22 V vs aqueous SCE, was used for derivatization. A 4.5 nm thick NAB multilayer was deposited by four scans between +400 and –600 mV vs Ag/Ag⁺ at 200 mV/s. A 1.9 nm thick NAB monolayer was deposited by cycling PPF once between +400 and –200 mV vs Ag⁺/Ag at a scan rate of 200 mV/s. Similarly, a 1.7 nm thick FL monolayer was deposited by cycling PPF once in the corresponding diazonium salt solution between +400 and –800 mV vs Ag⁺/Ag at a scan rate of 200 mV/s. As has been discussed by several authors,^{33,34,36,39} diazonium reduction can lead to multilayers via attack of the initial monolayer by subsequently electrogenerated radicals. To verify molecular layer thickness, AFM “scratching” was used as described in detail elsewhere.³³ Following surface modification, all the samples were immediately transferred to a clean filtered acetonitrile solution for 1 min to remove residual diazonium salt, then rinsed in acetonitrile, and dried with an argon stream.

Following surface derivation and cleaning, the modified samples were loaded into a vacuum chamber for metal deposition through a shadow mask consisting of four 0.5 mm wide parallel lines. The mask and the samples were positioned on a rotating holder ~50 cm from the crucible of an electron-beam source (Telemark,

- (25) Nowak, A. M.; McCreery, R. L. *Anal. Chem.* **2004**, *76*, 1089.
 (26) Nowak, A.; McCreery, R. *J. Am. Chem. Soc.* **2004**, *126*, 16621.
 (27) Liu, Y.-C.; McCreery, R. L. *Anal. Chem.* **1997**, *69*, 2091.
 (28) Liu, Y.-C.; McCreery, R. L. *J. Am. Chem. Soc.* **1995**, *117*, 11254.
 (29) Stewart, M. P.; Maya, F.; Kosynkin, D. V.; Dirk, S. M.; Stapleton, J. J.; McGuinness, C. L.; Allara, D. L.; Tour, J. M. *J. Am. Chem. Soc.* **2004**, *126*, 370.
 (30) Kariuki, J. K.; McDermott, M. T. *Langmuir* **2001**, *17*, 5947.
 (31) Kuo, T.-C.; McCreery, R. L. *Anal. Chem.* **1999**, *71*, 1553.
 (32) Allongue, P.; Delamar, M.; Desbat, B.; Fagebaume, O.; Hitmi, R.; Pinson, J.; Saveant, J. M. *J. Am. Chem. Soc.* **1997**, *119*, 201.
 (33) Anariba, F.; DuVall, S. H.; McCreery, R. L. *Anal. Chem.* **2003**, *75*, 3837.
 (34) Kariuki, J. K.; McDermott, M. T. *Langmuir* **1999**, *15*, 6534.
 (35) Brooksby, P. A.; Downard, A. J. *Langmuir* **2004**, *20*, 5038.
 (36) Combellas, C.; Kanoufi, F.; Pinson, J.; Podvorica, F. *Langmuir* **2005**, *21*, 280.
 (37) Ranganathan, S.; Steidel, I.; Anariba, F.; McCreery, R. L. *Nano Lett.* **2001**, *1*, 491.

- (38) Ranganathan, S.; McCreery, R. L.; Majji, S. M.; Madou, M. J. *Electrochem. Soc.* **2000**, *147*, 277.
 (39) Kiema, G. K.; Fitzpatrick, G.; McDermott, M. T. *Anal. Chem.* **1999**, *71*, 4306.

Freemont, CA). Metal deposition details are provided in the Supporting Information, Table 2S, with nominal film thicknesses determined by a Telemark 860 deposition controller with quartz crystal microbalance. The AlOx film thickness was verified with AFM "scratching"³³ on a sample lacking the Au and molecular layers to be 3.26 ± 0.036 nm. For PPF/molecule/TiOx/Au junctions, nominally 3.0 nm of titanium was deposited at 7×10^{-6} Torr, and the thickness of the resulting titanium oxide deposit was verified with AFM to be 3.13 ± 0.03 nm. A slightly different procedure was followed to produce PPF/molecule/TiO₂/Au junctions. After cryopumping to $<7 \times 10^{-6}$ Torr, 3 nm of Ti was deposited at 0.03 nm/s and the chamber was vented with air for 45 min and then reevacuated before a 7 nm Au deposition at 0.1 nm/s. The 45 min of exposure to air between Ti and Au depositions allowed the Ti to oxidize to titanium(IV) oxide, as indicated by XPS (see below). Other than the TiO₂ case, the junctions were not exposed to air until after Au deposition. In all cases, the gold layer both protected the Cu or metal oxide layers and yielded good electrical contact. The composition and oxidation states of the various junction structures are discussed below, but for the sake of labeling, "AlOx" refers to aluminum(III) oxyhydroxide, "TiOx" is a mixed titanium(II), titanium(III), and titanium(IV) oxide, and "TiO₂" designates a disordered form of TiO₂.

In situ Raman spectra of junctions under applied bias were obtained as described previously,²⁶ using a partially transparent top contact of Au(7.0)/AlOx(3.1) and a 0.07 cm² junction area, as indicated in the figures. A 514.5 nm laser was focused as a 50 $\mu\text{m} \times 5$ mm line at the junction (30 mW at the sample), and scattered light was collected by a custom spectrograph and Andor back thinned CCD detector.⁴⁰ After the bias was held at a given value for 30 s, Raman spectra were collected as the average of ten 2 s laser/CCD exposures. PPF spectra obtained separately were subtracted in all cases shown, and spikes in the spectra were removed by comparison of different 2 s spectra before averaging.

The junction area is defined by the intersection of the molecule-modified PPF strip (1 mm wide) and the Au/metal top contact (0.5 mm), for a junction area of 0.005 cm². Each sample was comprised of 8 or 12 crossed junctions. Each junction was contacted individually using three Au-plated Pt wires (MM Micromanipulator, Carson City, NV) positioned with three three-axis micropositioners. This "three-wire" configuration is analogous to the three electrodes typically used by potentiostats in electrochemical experiments,⁴¹ and corrects for ohmic potential losses in the PPF. Electronic testing was carried out with a Labview-based system using a National Instruments 6210 data acquisition board, with two A/D channels monitoring the current signal from a Keithley model 428 current amplifier and the *iR*-corrected applied voltage. In all cases, the voltage axis in the figures is PPF relative to Au. Except where noted, all experiments were carried out at room temperature within 1 day after fabrication.

Junction capacitance was measured with a Stanford Research SR720 LCR meter, using a four-wire geometry and frequencies of 0.1, 1, 10, and 100 kHz, or with cyclic voltammetry (*J* at $V = 0$ divided by the scan rate). The XPS analysis was performed with a Kratos Axis Ultra spectrometer equipped with a monochromated Al K α X-ray source. The base pressure of the analysis chamber was less than 1×10^{-9} Torr. A pass energy of 20 eV and step energy of 0.1 eV were used for all high-resolution acquisitions. Survey scans were collected using a pass energy of 80 eV and a step energy of 1 eV. The metal overlayers were sputtered with Ar⁺

ions, and XPS spectra were collected periodically. Integration and peak fitting were performed using the software provided with the Kratos instrument using a Shirley baseline and Gaussian–Lorentzian line shape (less than 50 iterations to achieve the lowest χ^2).

Results

Molecular junctions of NAB and FL of three types are compared in Figures 1–3: PPF/molecule/Cu/Au, PPF/molecule/TiO₂/Au, and PPF/molecule/AlOx/Au. Figure 1 shows overlays of *J/V* curves for PPF/NAB (4.5) junctions with Cu, TiO₂, and AlOx top contacts, all obtained at 100 V/s, and Figure 2 shows a similar set of *J/V* curves for PPF/FL (1.7) junctions. Tables 1 and 2 list the low-voltage ($V = \pm 0.1$) resistances, in terms of the product of observed resistance and junction area ($\Omega \text{ cm}^2$). Not surprisingly, the oxide junctions have much higher resistance than the Cu junctions. Moreover, the TiO₂ junctions exhibit much higher conductance than the AlOx analogues for high positive bias ($\sim 1 \text{ A/cm}^2$ at +3 V), and are rectifying, with $J(+2.5 \text{ V})/J(-2.5 \text{ V})$ of approximately 41. In our original publication on PPF/NAB(3.7)/TiOx(50)/Au junctions,^{20,21} we reported a low-voltage resistance of $4.1 \times 10^6 \Omega \text{ cm}^2$ and a current density at $V = +3$ of 0.75 A/cm^2 . The much lower resistance of the current junctions is presumably due to the much thicker TiOx layer used previously (53 nm compared to 3.1 nm).

As shown in Figure 3, the behavior of the PPF/molecule/TiO₂/Au junctions is strongly dependent on the structure and thickness of the molecular layer, with a fluorene(1.7) junction having an order of magnitude higher resistance and lower current densities than an NAB(1.9) junction. In all cases the FL(1.7)/TiO₂ and NAB(1.9)/TiO₂ junctions had approximately symmetric *J/V* curves, while NAB(4.5)/TiO₂ junctions were strongly rectifying. If the molecular layer is absent, the conductance of the PPF/TiO₂/Au junction is high and linear with applied *V* (shown in Figure 3), while the AlOx junction shows a high resistance and approximately ohmic behavior (Table 2). The low resistance of the PPF/TiO₂/Au control junction may indicate that the TiO₂ has residual electrons in its conduction band.

Junction capacitance was determined both from *J/V* curves, by dividing the current density at $V = 0$ by the scan rate, and with an LCR meter. As shown in Table 1, the capacitance is somewhat dependent on the scan rate for the AlOx junctions, decreasing by approximately 20% over a factor of 100 in frequency or scan rate. NAB(4.5)/TiO₂ junctions showed a similar trend, decreasing from 4.1 to 3.3 $\mu\text{F/cm}^2$ for a range of 10–250 V/s. NAB(1.9)/TiO₂ showed slightly greater variation with scan rate (from 11.3 to 8.0 $\mu\text{F/cm}^2$ for 100–250 V/s), but measurement error was larger in this case due to the difficulty of distinguishing the capacitive current from the relatively large resistive current. The high conductance of Cu junctions prevented accurate estimates of capacitance for the same reason. Table 2 summarizes the average capacitance from cyclic voltammetry for various junctions. The numbers of junctions and samples included in the averages are indicated in the second column of Table 2. A few junctions were rejected due to low resistance, but not more than 20% of a given junction type. For example, 7 out of a total of 38 PPF/NAB(4.5)/TiO₂(3.1)/

(40) Ramsey, J. D.; Ranganathan, S.; Zhao, J.; McCreery, R. L. *Appl. Spectrosc.* **2001**, *55*, 767.

(41) Bard, A. J.; Faulkner, L. R. *Electrochemical Methods*, 2nd ed.; Wiley: New York, 2001.

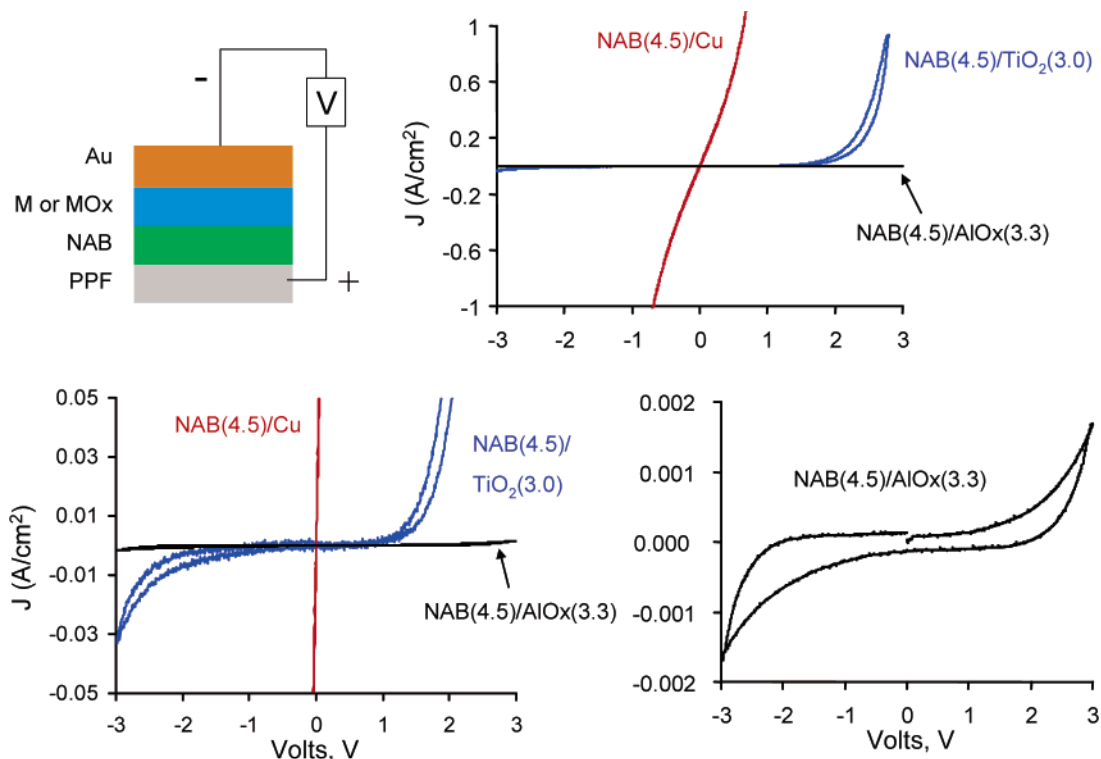


Figure 1. J/V curves for PPF/NAB(4.5) junctions with metal and metal oxide top contacts as indicated, plotted with three different current scales. Numbers in parentheses indicate the layer thickness in nanometers. The scan rate was 100 V/s in all the cases, and the junction area was 0.005 cm². Voltage on the x -axis is PPF relative to Au, and positive current density indicates electron flow through the junction from Au to PPF. In the schematic shown in the upper left, M and MOx represent Cu, AlOx, or TiO₂, as indicated for each J/V curve.

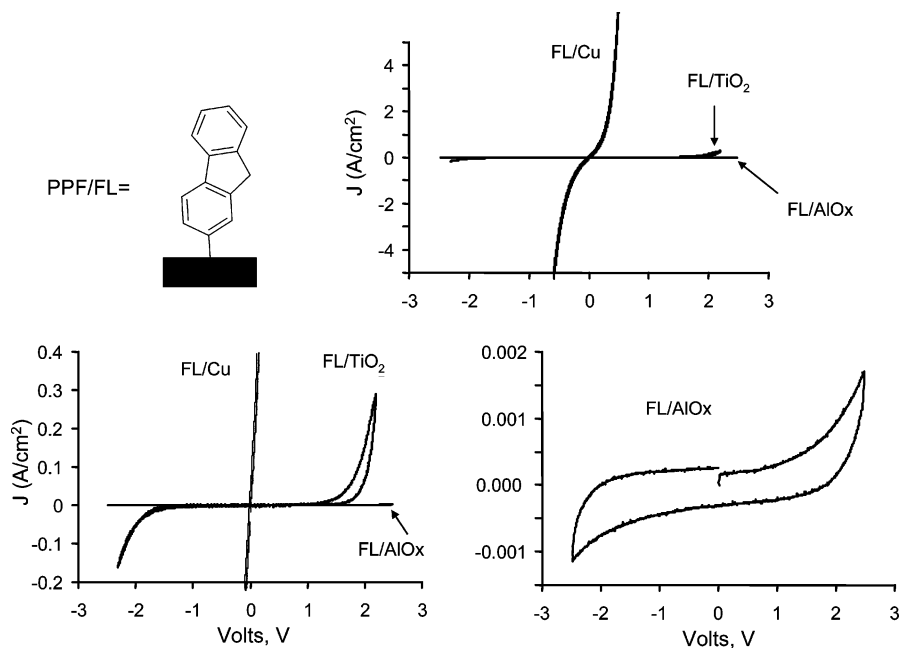


Figure 2. J/V curves for PPF/FL(1.7) junctions with metal and metal oxide top contacts as indicated, on three different current scales. Conditions are the same as in Figure 1.

Au junctions studied had resistances between 50 and 150 Ω cm², and were not included in the average.

As reported previously,²² the TiOx layer formed using a chamber pressure in the range of 2×10^{-7} to 8×10^{-6} Torr is a mixture of titanium(0) and titanium(II), titanium(III), and titanium(IV) oxides. The oxide level strongly affected the electronic behavior, but its effects were avoided by substituting Cu for Ti. Given the importance of oxides to junction behavior, the various junction configurations used

in the current work were examined with XPS depth profiling. In all cases, the metal or metal oxide layer was nominally 3.0 nm thick, and had a protective Au layer 7.0 nm thick. The XPS spectra shown in Figures 4 and 5 were obtained when the survey spectra indicated that Ar⁺ etching had progressed to the metal/molecule or metal oxide/molecule interface. Details of the XPS characterization and peak assignments (Table 2S) are provided in the Supporting Information, but the results are summarized here.

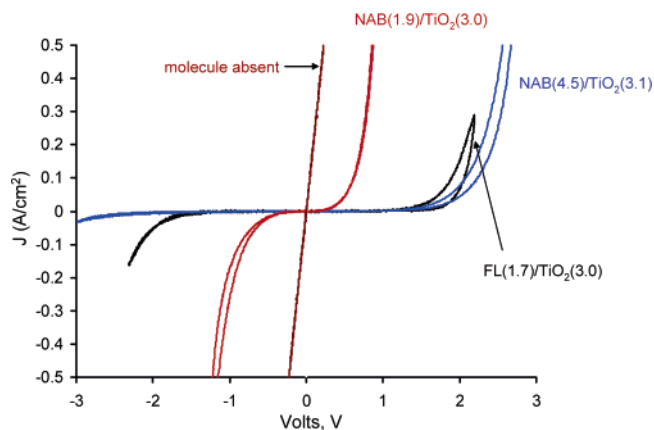


Figure 3. J/V curves for PPF/molecule/ $\text{TiO}_2(3.1)/\text{Au}$ junctions taken at a scan rate of 100 V/s. The molecular layer thickness as determined by AFM is shown in the parentheses in nanometers. The “molecule absent” curve is from a control junction prepared under identical conditions without the diazonium reduction step. Other conditions are the same as in Figure 1.

Table 1. Resistance and Capacitance for a PPF/NAB(4.5)/ $\text{AlOx}(3.3)/\text{Au}$ Junction

frequency, ^a Hz	scan rate, ^b V/s	capacitance, $\mu\text{F}/\text{cm}^2$	resistance, ^c $\Omega \text{ cm}^2$
	0.025		2.35×10^6
	0.10		1.41×10^6
	1.0		4.41×10^5
	10	1.57	1.92×10^4
	100	1.53	
	250	1.44	2.98×10^3
	1000		1.8×10^3
100	40	1.37	
1000	400	1.37	
10000	4000	1.27	

^a When a frequency is listed, the LCR meter was used, with 0.1 V amplitude. ^b For LCR the equivalent scan rate was assumed to be $4 \times \text{amplitude} \times \text{frequency}$. ^c For low voltage (<0.1 V); the entry is the product of the observed resistance and junction area.

Table 2. Observed Resistance and Capacitance for PPF/Molecule/Metal(Oxide)/Metal Junctions

junction	no. of junctions/ samples	capacitance, ^a $\mu\text{F}/\text{cm}^2$	resistance, ^b $\Omega \text{ cm}^2$
PPF/ $\text{AlOx}(3.3)/\text{Au}$	8/2 ^c	3.8 ± 0.3	1730 ± 170
PPF/ $\text{TiO}_2(3.1)/\text{Au}$	8/2	d	3.25
PPF/NAB(1.9)/ $\text{TiO}_2(3.1)/\text{Au}$	22/6	10.0 ± 1.8	56 ± 16
PPF/NAB(4.5)/ $\text{TiO}_2(3.1)/\text{Au}$	31/7	3.54 ± 0.5	371 ± 20
PPF/NAB(1.9)/ $\text{AlOx}(3.3)/\text{Au}$	7/2	3.11 ± 0.25	2620 ± 340
PPF/NAB(4.5)/ $\text{AlOx}(3.3)/\text{Au}$	9/3	1.42 ± 0.31	9620 ± 760
PPF/NAB(4.5)/ $\text{Cu}(3.0)/\text{Au}$	8/2	d	1.73 ± 0.13
PPF/FL(1.7)/ $\text{TiO}_2(3.1)/\text{Au}$	17/4	3.41 ± 0.42	218 ± 16
PPF/FL(1.7)/ $\text{AlOx}(3.3)/\text{Au}$	10/3	1.97 ± 0.29	8970 ± 490
PPF/FL(1.7)/ $\text{Cu}(3.0)/\text{Au}$		d	0.31^e

^a By cyclic voltammetry, mean of values for 10–250 V/s. ^b By cyclic voltammetry, scan rate of 10 V/s, $V = \pm 0.05$ V, product of observed resistance and junction area (0.005 cm^2). ^c Denotes eight junctions from two samples. ^d Resistive current too large to permit capacitance measurement. ^e From ref 17, average for three FL(1.7) samples, all with 30 nm of Cu rather than 3.0 nm.

High-resolution scans of the NAB/ AlOx interfacial region are shown in Figure 4, as are those from FL/ Cu junctions. The single Al_{2p} peak observed at 75.4 eV can be assigned to either Al_2O_3 or $\text{Al}(\text{OH})_3$, and no Al^0 was detected. There is no evidence for the formation of an Al–N bond between the vapor-deposited Al and the NO_2 groups in the NAB layer, due to the absence of an Al_{2p} peak at ~ 74.5 eV^{42,43} and an N_{1s} peak at ~ 397 eV.^{44–46} As discussed in detail in the Supporting Information, the XPS results clearly establish that

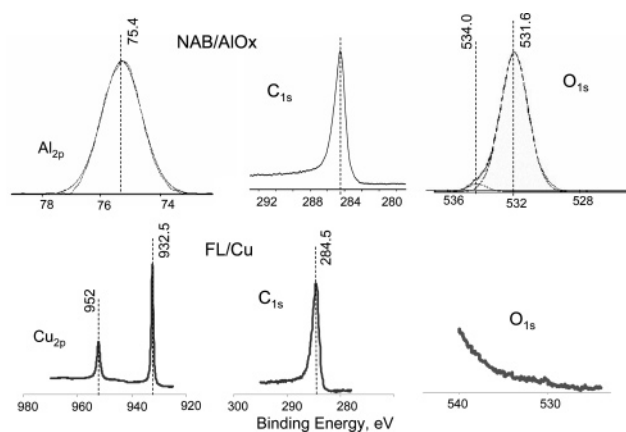


Figure 4. XPS spectra of the Al_{2p} , C_{1s} , and O_{1s} regions of the PPF/NAB(1.9)/ $\text{AlO}_x(3.3)/\text{Au}$ junction following Ar^+ sputtering to a region near the NAB/ AlO_x interface (upper three spectra). The lower three spectra show the Cu_{2p} , C_{1s} , and O_{1s} regions of a PPF/FL(1.7)/ $\text{Cu}(3.0)/\text{Au}$ junction near the FL/ Cu interface. Ar^+ sputtering was done in both the cases to remove most of the Au, Al, and Cu overlayers, so that the composition reflects that near the molecular layer.

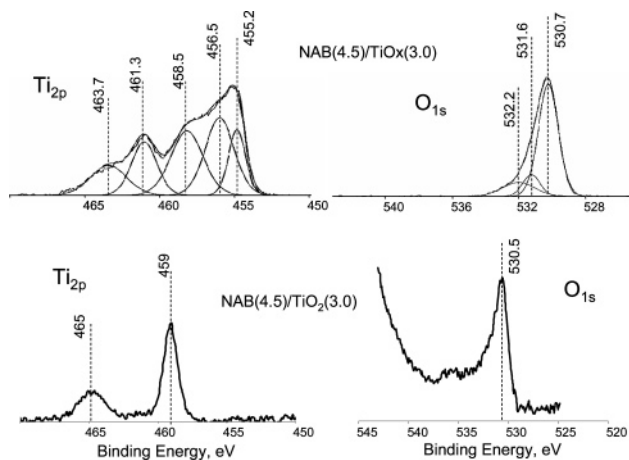


Figure 5. XPS spectra of the Ti_{2p} and O_{1s} regions of the PPF/NAB(4.5)/ $\text{TiO}_x(3.1)/\text{Au}$ (upper) and PPF/NAB(4.5)/ $\text{TiO}_2(3.1)/\text{Au}$ (lower) junctions. For the TiO_2 case, the Ti deposit was exposed to air before Au deposition, as noted in the Experimental Section and Table 1S in the Supporting Information.

the Al layer is Al^{III} , mostly as hydroxide, which does not appear to interact strongly with the NAB layer.

The lower row of spectra in Figure 4 were obtained near the fluorene/ Cu interface in a PPF/FL(1.7)/ $\text{Cu}(3.0)/\text{Au}$ junction following Ar^+ sputtering. At no point after the initiation of depth profiling was oxygen detected for the PPF/FL/ Cu/Au junction. The high-resolution spectrum of the Ti_{2p} and O_{1s} regions of NAB(4.5)/ TiO_x junctions made with different Ti deposition conditions are shown in Figure 5. The upper spectra in Figure 5 were obtained with the “ TiO_x ” conditions in which the Ti was not exposed to air before Au deposition. As described in the Supporting Information, the TiO_x layer

(42) *Practical Surface Analysis*, 2nd ed.; Vol. 1: Auger and X-ray Photoelectron Spectroscopy; Briggs, D., Seah, M. P., Eds.; John Wiley and Sons: Chichester, U.K., 1990.

(43) Ning, J.; Xu, S.; Ostrikov, K. N.; Chai, J.; Li, Y.; Koh, M. L.; Lee, S. *Thin Solid Films* **2001**, *385*, 55.

(44) Liao, H. M.; Sodhi, R. N. S.; Coyle, T. W. *J. Vac. Sci. Technol., A* **1993**, *11*, 2681.

(45) Zhang, J.; Anson, F. C. *J. Electroanal. Chem.* **1992**, *331*, 945.

(46) Katnani, A. D.; Papathomas, K. I. *J. Vac. Sci. Technol., A* **1987**, *5*, 1335.

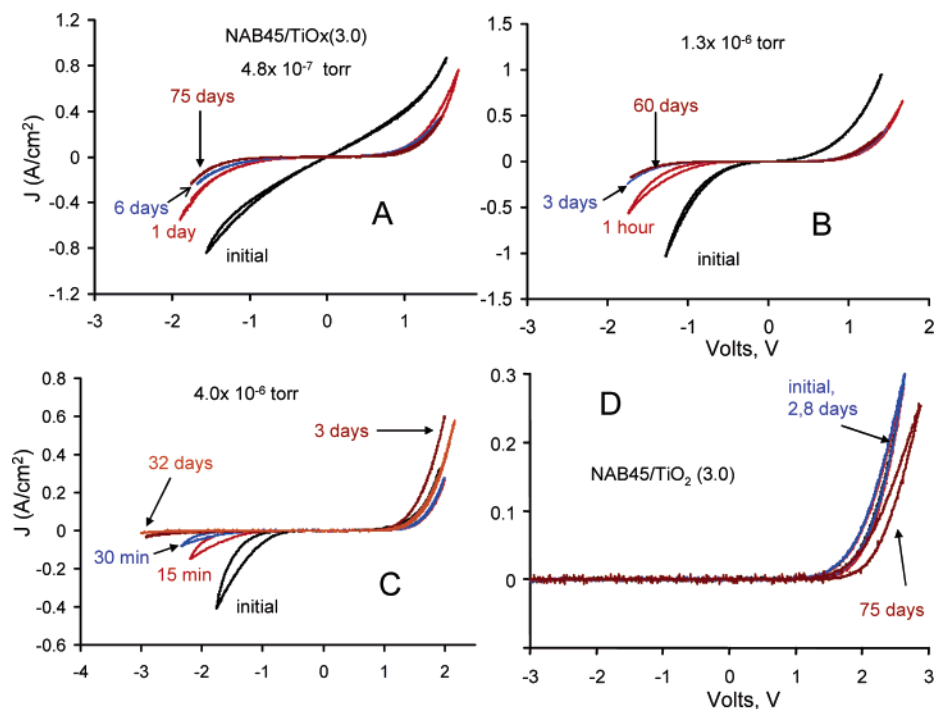


Figure 6. J/V curves for PPF/NAB(4.5)/TiO_x(3.1)/Au junctions prepared with TiO_x/Au top contact deposited at 4.8×10^{-7} (A), 1.3×10^{-6} (B), and 4.0×10^{-6} (C) Torr. Panel D shows the J/V curves for the carbon/NAB(4.5)/TiO₂(3.1)/Au junction made by opening the chamber between Ti and Au depositions. In all the cases, J/V curves were recorded at a scan rate of 100 V/s and at various times after the junctions were made, as indicated.

consisted of Ti₂O₃ (~42% of total Ti), TiO₂ (~34%), and either Ti–N or Ti–O (~24%). Two peaks were observed in the N_{1s} region, which correspond to the N=N group in the NAB layer (399.3 eV)²⁷ and the Ti–N bond between the NO₂ group and the titanium top contact (397.1).^{25,47–49} The formation of this covalent Ti–N bond was established in a previous study,²⁵ and implies a molecular junction with covalent bonds at both the Ti/NAB and PPF/NAB interfaces.

As noted previously,²² reduction of back-pressure during Ti deposition reduces, but does not eliminate, titanium oxides, at least for the minimum back-pressure available with the apparatus used (2×10^{-7} Torr). However, increasing the pressure and exposing the Ti deposit to air results in a Ti layer which is predominately TiO₂. The lower spectra of Figure 5 were obtained from a PPF/NAB(4.5)/TiO₂(3.1)/Au junction after Ar⁺ etching to reach the NAB/Ti interface. All observable Ti is present as Ti^{IV}, and the O_{1s} spectrum corresponds to metal oxide rather than hydroxide. Whenever Ti junctions are discussed below, they have been prepared such that Ti occurs as TiO₂, unless noted otherwise. XPS of PPF/NAB(4.5)/Cu/Au junctions (data not shown) indicated low levels of oxygen at the copper/molecule interface, some of which originated in the NAB nitro group.

Given the variation in titanium oxide composition with deposition conditions, the electronic properties of PPF/NAB(4.5)/TiO_x(3.1)/Au junctions were examined as a function of deposition pressure and time after exposure to air. As shown in Figure 6A, a newly formed junction made at 5×10^{-7} Torr had relatively high conductivity, approaching that

observed with a Cu top contact. The J/V curve changed with time in air until it stabilized within approximately 24 h. As shown in Figure 6B, a higher deposition pressure results in higher initial resistance, which also increases for about 24 h after exposure to air. For deposition at 4×10^{-6} Torr (Figure 6C), the J/V curve is initially symmetric but within a few hours becomes rectifying. Although the shape and symmetry of the J/V curves for low deposition pressure depend on both the deposition pressure and exposure to air, an intentionally oxidized junction containing predominantly TiO₂ is rectifying and stable to air exposure (Figure 6D). Combined with the XPS results (Figure 5), we conclude that rectification occurs when TiO₂ is the dominant titanium oxide. Furthermore, junctions which initially contain Ti^{II} and Ti^{III} tend to form TiO₂, presumably by reaction with residual water or O₂ in the junction and more slowly by air exposure of a completed junction over several weeks.

We reported previously on the use of in situ Raman spectroscopy to monitor structural changes within PPF/NAB(4.5)/TiO_x/Au junctions under applied bias.²⁶ The same approach was used to investigate structural changes under bias for the NAB/AlO_x junctions in the present work. Figure 7 shows spectra of a PPF/NAB(4.5)/AlO_x(3.3)/Au junction for a bias range of +1.0 to –1.5 V; larger positive voltages caused irreversible loss of the entire spectrum and were avoided. Note that the relative intensities of the 1401 and 1448 cm^{–1} bands vary with the applied bias, and these changes were reversible for at least two voltage cycles between +1.0 and –1.5 V. The changes are more evident in plots of the ratio of the 1401 to 1448 cm^{–1} peak intensities vs bias for three separate junctions shown in Figure 8. Figure 9 shows that when a more negative bias is applied, the spectrum exhibits dramatic changes, with a reversible loss

(47) Badrinarayanan, S.; Sinha, S.; Mandale, A. B. *J. Electron Spectrosc. Relat. Phenom.* **1989**, *49*, 303.

(48) Biwer, B. M.; Bernasek, S. L. *Surf. Sci.* **1986**, *167*, 207.

(49) Shul'ga, Y. M.; Troitskii, V. N.; Aivazov, M. I.; Borodk'o, Y. G. *Zh. Neorg. Khim.* **1976**, *21*, 2621.

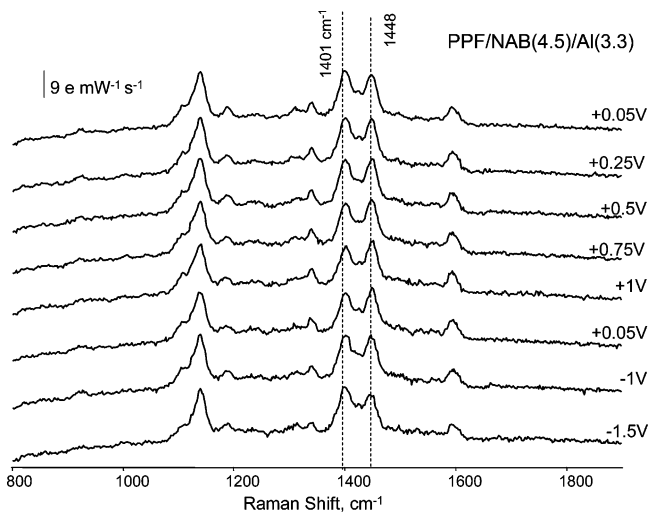


Figure 7. In situ Raman spectra of a PPF/NAB(4.5)/AlO_x(3.3)/Au(7.0) junction as a function of the applied bias. The junction area was 0.07 cm², and the spectra progressed from top to bottom in the order shown.

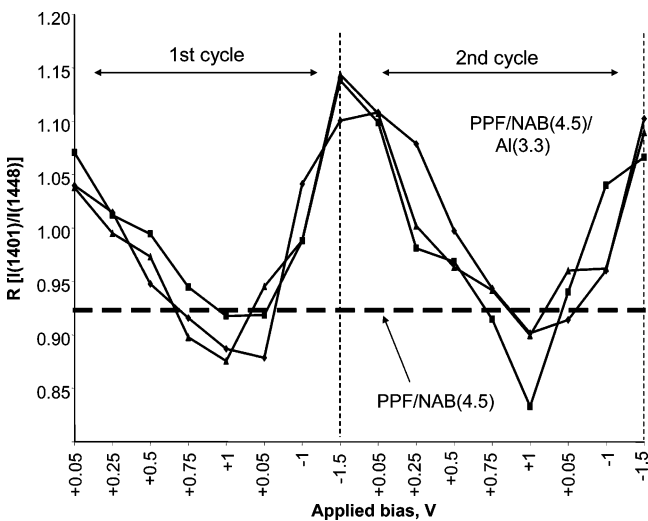


Figure 8. Ratio of 1401 to 1448 cm⁻¹ Raman band intensity as a function of bias for PPF/NAB(4.5)/AlO_x(3.3)/Au junctions, for a series of spectra similar to those in Figure 7. Three trials on independent junctions are shown, and the horizontal line is the ratio observed for NAB(4.5) on PPF before metal deposition.

of all peaks at -3 V and irreversible changes in the shapes and intensities of the 1340, 1401, and 1448 cm⁻¹ bands. Fluorene is not a sufficiently strong Raman scatterer to obtain an in situ spectrum with the present apparatus, and the weak spectrum from NAB(1.9)/Ti(3.1) junctions prevented unequivocal observation of structural changes. Raman spectroscopy of Cu junctions was attempted, but their very high conductance and large area prevented observation of meaningful i/V curves, or any changes in the Raman spectrum with the applied bias.

Discussion

An obvious initial concern is verifying the structures and compositions of the various junctions. The lack of detectible oxygen in the PPF/FL/Cu/Au junction indicates minimal formation of copper oxide during Cu deposition or upon exposure of the completed Cu junction to air. As reported previously, PPF/molecule/Cu/Au junctions are stable at least several weeks after exposure to air, although there is a

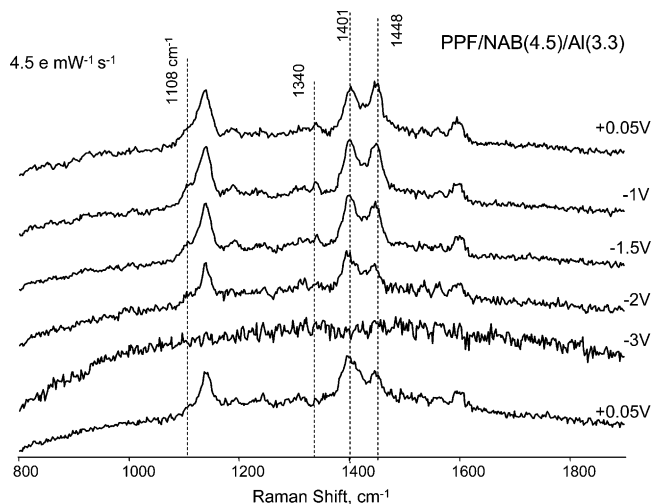


Figure 9. In situ Raman spectra of a PPF/NAB(4.5)/AlO_x(3.3)/Au junction for negative bias. The junction area was 0.07 cm², and the spectra progressed from top to bottom in the order shown.

gradual increase in resistance over a period of several months.^{17,22} The PPF/molecule/Al/Au junctions were formed under conditions which intentionally resulted in aluminum(III) oxide. The XPS results indicate a disordered oxyhydroxide, which will be referred to as “AlO_x”. The electronic behavior of the Al junctions was quite stable with air exposure after fabrication. While the Cu and Al junctions were well defined in terms of metal oxidation state, the Ti junctions varied greatly with the preparation conditions, ranging from a complex mixture of titanium(0) and titanium(II), titanium(III), and titanium(IV) oxides to predominantly TiO₂. The evolution of electronic properties with oxide content shown in Figure 6 may be useful for achieving different electronic characteristics, but for the current discussion, it is best to simplify junction composition as much as possible. Therefore, the electronic behaviors in Figures 1–3 were obtained with the conditions yielding only TiO₂ as the observable titanium oxide. Although the XPS of the Ti^{IV} deposit matches that of TiO₂, the film is likely to be disordered and possibly contain small amounts of residual water or hydroxide ion. For simplicity, we will refer to junctions made with exposure to air during Ti deposition as “PPF/molecule/TiO₂(3.1)/Au”, but it should be kept in mind that the TiO₂ is disordered. Junctions containing mixtures of Ti^{II}, Ti^{III}, and Ti^{IV} will be designated “TiO_x”.

The fact that the behavior of molecule/Ti junctions is so sensitive to the Ti^{IV} content is due to the conductivities of the various Ti oxidation states, as noted previously.^{22,26} Ti⁰, titanium(II) oxide, and titanium(III) oxide have resistivities ranging from 40 to 300 μΩ cm,^{50–52} while TiO₂ has a resistivity of ~10¹⁰ μΩ cm.⁵³ Stated differently, titanium(II) and titanium(III) oxides have electrons in the conduction band, while titanium(IV) oxide does not, making the sub-

(50) Mardare, D.; Baban, C.; Gavrile, R.; Modreanu, M.; Rusu, G. I. *Surf. Sci.* **2002**, 507–510, 468.

(51) Grigorov, K. G.; Grigorov, G. I.; Drajeva, L.; Bouchier, D.; Sporken, R.; Caudano, R. *Vacuum* **1998**, 51, 153.

(52) Leung, C.; Weinert, M.; Allen, P. B.; Wentzcovitch, R. M. *Phys. Rev. B* **1996**, 54, 7857.

(53) Weast, R. C. *CRC Handbook of Chemistry and Physics*, 66th ed.; CRC Press: Boca Raton, FL, 1985.

oxides relatively good electronic conductors. Alumina not only has a much higher band gap than TiO₂, but also lacks intermediate oxidation states between 0 and +3. The relationship between the conductivity of the molecular junction and the oxide composition is discussed in more detail below.

The observed capacitance of 3.8 $\mu\text{F}/\text{cm}^2$ for a PPF/AlOx-(3.3)/Au junction without NAB or FL present yields a dielectric constant for AlOx of 14, on the basis of a simple parallel plate model. Reported values for Al₂O₃ thin films are in the range of 7–11,^{54–57} but the AlOx film in the current work is at least partially hydrated, and may have a dielectric constant higher than that of Al₂O₃. When a molecular layer is present between the PPF and AlOx, the capacitance decreases, as expected for a parallel plate capacitor, and the thicker NAB(4.5) layer yields a lower capacitance than the NAB(1.9) case. The dielectric constant of TiO₂ varies significantly with microstructure and composition, but reported values are in the range of 50–110. It should be noted that the capacitances reported here are significantly higher than the $\sim 1 \mu\text{F}/\text{cm}^2$ reported previously for NAB-(3.7)/TiOx(5.3) junctions,^{20,21} due to the much thinner TiOx layer in the current work. Inspection of Table 2 reveals that replacing AlOx with TiO₂ significantly increases the junction capacitance, as expected from their dielectric constants. All else being equal, the FL junctions have lower capacitance than NAB junctions. Given the uncertainties of the dielectric constants of both oriented molecules and disordered metal oxides, the capacitance results do not unequivocally confirm the model of a well-stratified junction structure. However, the fact that the observed capacitances are reasonable is consistent with a parallel plate capacitor model with two distinct dielectric layers.

With regard to junction resistance, the three materials used as top contacts yield junctions of three distinct types. Cu and aluminum(III) oxide represent the extremes of highly conductive and quite insulating junctions, with resistances that differ by 3–4 orders of magnitude for a given molecular layer. Several PPF/molecule/Cu junctions were discussed in more detail elsewhere, and the i/V curves were found to depend strongly on the molecular structure and layer thickness.¹⁷ The focus here is on the combination of a molecular layer and the metal oxide, and the dramatic increase in resistance caused by the oxide. Since aluminum(III) oxide is an insulator (band gap 8.7 eV),⁵⁸ it is not surprising that a 3.3 nm layer greatly increases the resistance. Addition of a molecular layer has a relatively small effect on the resistance of AlOx junctions, with 4.5 nm of NAB increasing the resistance by a factor of 5.6. On the current scale relevant to Cu and TiO₂ junctions, the AlOx junctions are insulating, whether a molecular layer is or is not present.

The TiO₂ junctions have an intermediate low-voltage resistance compared to the Cu and AlOx junctions, but more

importantly, show much larger currents than the AlOx junctions for positive bias excursions. TiO₂ has a much smaller band gap than AlOx (~ 3.0 vs 8.7 eV),^{54,59} and its semiconducting nature is the likely source of the dramatic differences from Cu and AlOx evident in Figures 1 and 2. On the basis of spectroscopic evidence in active PPF/NAB-(4.5)/TiOx/Au junctions, we proposed that a positive applied bias (making the TiOx negative) can inject electrons into the TiOx conduction band, generating charge carriers and decreasing the resistance of the TiOx layer.²⁶ Apparently the low conductivity of AlOx at any accessible voltage yields low junction conductivity for all the AlOx junctions studied. The role of possible counterions, such as H⁺ or OH⁻, is unclear, although they may be required for a redox process to occur if local electroneutrality is conserved. Although mobile ions were not intentionally included in the junction design, they may result from reactions of vapor-deposited metals with residual water or oxygen. An additional concern reported by several laboratories in the literature is damage to the molecular layer from Ti metal deposition.^{60–65} We have shown previously that the Raman spectrum of an NAB layer is not destroyed by Ti deposition, and that the resulting junction exhibits both conductance and spectroscopic changes under bias.^{21,25,26} Furthermore, the behavior of TiO₂ junctions reported here cannot be solely due to monolayer damage, or the FL and NAB junctions would not differ substantially in their electronic behavior. It is likely that the Ti metal rapidly reacts with water or oxygen in our deposition conditions, which may prevent carbide formation and monolayer damage.

The Raman spectroscopy results provide important clues to what factors control junction behavior, since they provide unequivocal evidence for changes in molecular structure under bias. The NAB(4.5)/AlOx(3.3) junctions show spectral changes even though there is very low junction current. It should be noted that the current required for NAB reduction (a few $\mu\text{A}/\text{cm}^2$) is much smaller than the resistive or capacitive currents observed. The spectral changes in NAB-(4.5)/AlOx(3.3) junctions are qualitatively similar to those reported previously²⁶ for NAB(4.5)/Ti(1.0) and NAB(4.5)/Ti(3.1) junctions, but occur at less extreme bias. These spectral changes have been shown to correspond to reduction of NAB to a radical anion or “methide”, by analogy to electrochemical experiments in solution.^{26,66} The current results indicate that NAB is reduced when the PPF substrate is negative, although the AlOx layer blocks significant junction conductance. NAB is resonance Raman active on

- (54) Gusev, E. P.; Cartier, E.; Buchanan, D. A.; Gribelyuk, M.; Copel, M.; Okorn-Schmidt, H.; D'Emic, C. *Microelectron. Eng.* **2001**, *59*, 341.
 (55) Voigt, M.; Sokolowski, M. *Mater. Sci. Eng., B* **2004**, *B109*, 99.
 (56) Segda, B. B.; Jacquet, M.; Besse, J. P. *Vacuum* **2001**, *62*, 27.
 (57) Groner, M. D.; Elam, J. W.; Fabreguette, F. H.; George, S. M. *Thin Solid Films* **2002**, *413*, 186.
 (58) Ohuchi, F. S.; French, R. H. *J. Vac. Sci. Technol., A* **1987**, *6*, 1695.

- (59) Umebayashi, T.; Yamaki, T.; Itoh, H.; Asai, K. *Appl. Phys. Lett.* **2002**, *81*.
 (60) Konstadinidis, K.; Zhang, P.; Opila, R. L.; Allara, D. L. *Surf. Sci.* **1995**, *338*, 300.
 (61) Fisher, G. L.; Hooper, A. E.; Opila, R. L.; Jung, D. R.; Allara, D. L.; Winograd, N. *J. Phys. Chem. B* **2000**, *104*, 3267.
 (62) Fisher, G. L.; Walker, A. V.; Hooper, A. E.; Tighe, T. B.; Bahnck, K. B.; Skriba, H. T.; Reinard, M. D.; Haynie, B. C.; Opila, R. L.; Winograd, N.; Allara, D. L. *J. Am. Chem. Soc.* **2002**, *124*, 5528.
 (63) Haynie, B. C.; Walker, A. V.; Tighe, T. B.; Allara, D. L.; Winograd, N. *Appl. Surf. Sci.* **2003**, *203–204*, 433.
 (64) Walker, A. V.; Tighe, T. B.; Haynie, B. C.; Uppili, S.; Winograd, N.; Allara, D. L. *J. Phys. Chem. B* **2005**, *109*, 11263.
 (65) Boer, B. d.; Frank, M. M.; Chabal, Y. J.; Jiang, W.; Garfunkel, E.; Bao, Z. *Langmuir* **2004**, *20*, 1539.
 (66) Itoh, T.; McCreery, R. L. *J. Am. Chem. Soc.* **2002**, *124*, 10894.

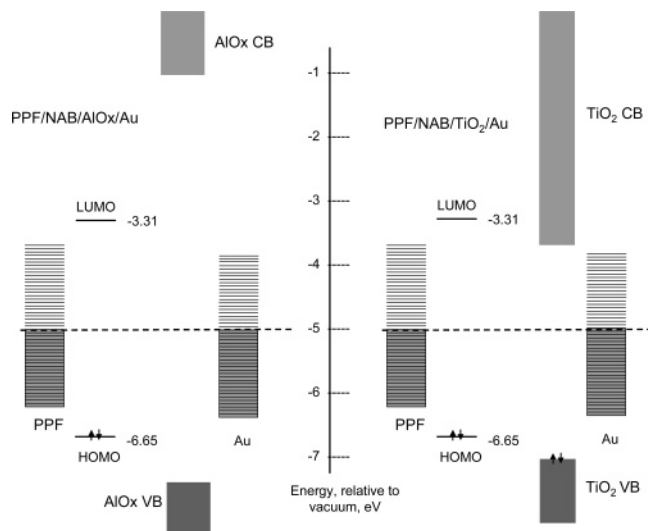


Figure 10. Vacuum-referenced energy levels for isolated materials comprising PPF/NAB junctions with AIOx/Au (left) and TiO₂/Au (right) top contacts. NAB energy levels are from DFT calculations (B3LYP-631G-(d)). The large band gap of AIOx is apparent from the significant energy difference between its conduction and valence band edges. The dashed horizontal line represents the assumed junction Fermi level. Note that molecular levels may be perturbed significantly by interaction with the contacts and oxides.

PPF, and the reversible disappearance of the NAB spectrum at -3 V is likely caused by a shift of the resonance Raman excitation profile away from the laser wavelength. In contrast, the NAB(1.9)/TiO₂(3.1) junctions show much larger currents than both the NAB(4.5)/TiO₂(3.1) and NAB(1.9)/AIOx(3.3) cases, but no spectroscopic changes were observed with the thinner NAB layer. The main conclusion from the Raman results is that NAB is reduced when the PPF is sufficiently negative, but only for a 4.5 nm NAB thickness accompanied by a TiOx or AIOx oxide layer, of the conditions investigated so far. There is no obvious change in electronic behavior accompanying NAB reduction in the NAB/AIOx junctions because the AIOx effectively blocks conduction through the junction. However, NAB reduction has a significant effect on conductance for the NAB/TiO₂ junctions, for reasons outlined in the next section.

A reasonable postulate which accounts for the observations can be formulated in the context of the vacuum-referenced energy levels for NAB and TiO₂ shown in Figure 10, shown for isolated materials. When the junction is formed, charge transfer between layers will cause realignment of these energy levels to an unknown extent, but there is general agreement that the junction Fermi level will remain between the HOMO and LUMO of the molecule, as shown. For the sake of discussion, we assume that the Fermi level is -5 V relative to a vacuum, approximately equal to the PPF and Au work functions. The AIOx is represented by the large band gap between its conduction and valence bands (~ 8 V), and it acts as an apparently insurmountable barrier to electron transfer, with the small currents observed in the AIOx junctions presumably due to field emission or defects. However, the NAB in an AIOx junction is redox active, forming reduced NAB when the PPF is negative. This redox activity does little for conduction, however, since the AIOx barrier is too high. When Cu is substituted for AIOx, the current increases by about 7 orders of magnitude, although

the i/V behavior remains symmetric. The NAB layer is a relatively good electronic conductor between Cu and PPF contacts, implying that the low currents observed for AIOx junctions result solely from the insulating properties of AIOx. As expected, a junction containing only AIOx(3.3) has a resistance nearly as high as that for NAB(1.9)/AIOx(3.3) and 3 orders of magnitude higher than that for NAB(1.9)/Cu.

PPF/NAB(4.5)/TiO₂(3.1)/Au not only has much lower conductance than the NAB(1.9) analogue, but also shows rectification. The higher resistance at low bias is presumably a consequence of the thicker molecule/TiO₂ barrier, 7.5 nm rather than 4.9 nm. It is likely that the high currents above $+2$ V occur when the Au Fermi level enters the conduction band of TiO₂, in which case the TiO₂ layer becomes conducting, and the current increases rapidly. As noted earlier, the differential conductance approaches that of the NAB(4.5)/Cu case when the bias is above 2 V, as expected once the conduction band is reached. In fact, the current density of ~ 1 A/cm² at a bias of ~ 3 V in the current PPF/NAB(4.5)/TiO₂(3.1)/Au junctions is comparable to that observed for a much thicker TiOx layer (0.75 A/cm² in PPF/NAB(3.7)/TiOx(53)/Au junctions).^{20,21} The weak dependence on TiOx thickness for $V > +2$ V is consistent with low-resistance transport in the TiOx conduction band. The low current for negative bias in NAB(4.5)/TiO₂(3.1) junctions may be caused by generation of a Coulombic barrier by reduction of NAB. The Raman spectra establish clearly that reduction of NAB occurs, and the resulting negative space charge may block further electron injection at negative bias. Alternatively, reduction of the NAB layer may deplete carriers from the TiO₂, thus increasing its resistance. The symmetry of the i/V curves for NAB(1.9)/TiO₂(3.1) junctions may imply that the thinner NAB layer conducts electrons at too fast a rate to permit significant buildup of anionic charge. It is possible that the high currents for the thinner junctions reduce the electric field across the NAB layer, thus decreasing the driving force for reduction.

The HOMO–LUMO gap of FL (5.03 eV) is larger than that of NAB (3.62 eV), which may account for the lower currents observed for FL/TiO₂ junctions compared to NAB/TiO₂ junctions of similar thickness (Figure 3). The applied bias would need to be larger for the Au Fermi level to reach the FL LUMO, which is also within the TiO₂ conduction band. Of course, arguments based on relative energies depend on the alignment of the Fermi levels of the contacts and the orbital energies of the molecules, as well as the shape of the electric field distribution within the junction. For example, the local electric field at the Au/TiO₂ interface can determine whether a mechanism based on tunneling or on electron injection into the conduction band is more likely.

Conclusions

Significant questions remain about the mechanisms of rectification and electron transport in PPF/molecule/metal junctions, but the current results permit several useful conclusions. First, TiO₂ is a necessary but not sufficient requirement for rectification, since PPF/TiO₂/Au junctions show symmetric J/V curves with high current (Figure 3). Therefore, Schottky barriers at the TiO₂/Au or PPF/TiO₂

interfaces cannot be solely responsible for rectification. Second, the composition of the titanium oxide layer can have drastic effects on the junction behavior, since the suboxides are conducting compared to TiO_2 , and can support redox reactions. Third, the J/V behavior of PPF/molecule/ TiO_2 /Au junctions is strongly dependent on the molecular structure and thickness, indicating a major molecular component in junction electronic properties. Fourth, reduction of the NAB-(4.5) layer is observed in either TiO_2 or AlOx junctions, despite large differences in the observed currents. It is possible that reduction occurs when the low conductivity caused by the oxides creates a large enough applied electric field to drive NAB reduction. Fifth, instrumental sensitivity prevented observation of NAB reduction in NAB(1.9) or FL-(1.7) junctions, so reduction in these cases cannot be ruled

out. Finally, the association of rectification with NAB reduction is likely a consequence of generation of a Coulombic barrier for negative bias; however, other explanations are possible.

Acknowledgment. This work was supported by the National Science Foundation through Project 0211693 from the Analytical and Surface Chemistry Division, and by ZettaCore, Inc. The XPS instrument was purchased with an NSF instrumentation grant, NSF-DMR 0114098.

Supporting Information Available: Detailed discussion of XPS results including tables and references (PDF). This material is available free of charge via the Internet at <http://pubs.acs.org>.

CM050689C